

Voids in the Simulated Local Universe

H. Mathis^{1*} and S. D. M. White¹

¹*Max-Planck-Institute for Astrophysics, D-85741 Garching, Germany*

31 October 2018

ABSTRACT

We use simulations of the formation and evolution of the galaxy population in the Local Universe to address the issue of whether the standard theoretical model succeeds in producing empty regions as large and as dark as the observed nearby ones. We follow the formation of galaxies in a Λ CDM universe and work with mock catalogues which can resolve the morphology of LMC sized galaxies, and the luminosity of objects 6 times fainter. We look for a void signature in sets of virialized haloes selected by mass, as well as in mock galaxy samples selected according to observationally relevant quantities, like luminosity, colour, or morphology. We find several void regions with diameter $10h^{-1}$ Mpc in the simulation where gravity seems to have swept away even the smallest haloes we were able to track. We probe the environment density of the various populations and compute luminosity functions for galaxies residing in underdense, mean density and overdense regions. We also use nearest neighbour statistics to check possible void populations, taking L_* spirals as reference neighbours. Down to our resolution limits, we find that all types of galaxies avoid the same regions, and that no class appears to populate the voids defined by the bright galaxies.

Key words: large-scale structure of the Universe – galaxies: statistics – galaxies: formation

1 INTRODUCTION

Early concerns about the existence of a hypothetical, spatially homogeneous population of galaxies may be traced back to the negative conclusions of Soneira & Peebles (1977), well before it was realized that the local universe contains huge regions apparently empty of normal, optically selected galaxies (Kirshner et al. 1981). More recent observations targetted specific classes of galaxy (e.g. dwarfs, low surface brightness or star-forming galaxies) finding that the optically-defined voids also seem strongly underdense in all these objects (see Section 2 of Peebles 2001 for a list of observations). There have been reports of the detection of some galaxies in previously defined voids, like Boötes (Dey et al. 1990; Szomoru et al. 1996ab), but these are mostly normal, late-type spirals near the edge of the void region. Starting from a morphology density relation like that of Dressler (1980), one might expect the voids to be populated by a population of dwarf, faint galaxies. However, even these populations are not observed. As noted by Kirshner et al. (1981) and underlined by Peebles (2001, hereafter P01), *if* there is still substantial mass in the voids, the galaxies associated with DM haloes in the voids must be several magnitudes fainter than L_* . The Magellanic-type irregulars close to the

Local Group (Tully 1988; Peebles 1989; Peebles et al. 2000) seem to have formed in conditions quite comparable to those occurring in the voids so one might expect to find the same type of galaxy there.

Given that the same large underdense regions are observed in different surveys and populations, several groups have recently focused on the precise determination of the sizes and shapes of voids in large redshift surveys, like the *CfA* redshift survey (Vogeley et al. 1994), the *LCRS* (Müller et al. 2000; Müller & Arbabi-Bidgoli 2001), the *SSRS* and *IRAS* surveys (El-Ad et al. 1997; El-Ad & Piran 1997), and the *PSCz* survey (Plionis & Basilakos 2001). When comparing the voids in the *IRAS* 1.2 Jy survey and in the *ORS*, El-Ad & Piran (2000) found similar sizes and shapes, although the galaxy populations are very different in the two samples.

Some authors (White et al. 1987; Vogeley et al. 1994; Müller et al. 2000; Plionis & Basilakos 2001) have used simulations of the dark matter distribution in CDM models to compare to observations of “voids”. All of this work identified galaxy sites by simple statistical bias models rather than by *ab initio* galaxy formation modelling. Many authors also studied regions too small to provide reliable statistics. Vogeley et al. (1994) found that biased models (e.g. a flat, low-density CDM cosmology) generally produce voids that are similar to the observations in the *CfA* survey when consider-

* Email: hmathis@mpa-garching.mpg.de

ing bright galaxies, but which are too empty when including fainter galaxies. Müller et al. (2000) found their void statistics to be more sensitive to the criterion for galaxy identification than to the cosmological parameters themselves. Plionis & Basilakos (2001) compared the void shapes and sizes in the *PSCz* with six different CDM models. They found the distribution of void sizes to differ strongly between models. Models with high σ_8 like OCDM and Λ CDM provided the best fits.

The main drawback of these kinds of simulations is the necessity to put in the galaxies “by hand”, using an *ad hoc* bias recipe, and/or by assigning morphologies using the observed morphology-density relation.

In recent years, numerical simulations of structure formation in cosmological volumes have been extended in two different ways to include an explicit treatment of galaxy formation by means of semi-analytic techniques. In the faster, but less direct technique, galaxies are inserted in each dark halo at the time of observation based on a Monte-Carlo realization of the merging and galaxy formation history of a “random” halo of similar mass (Kauffmann et al. 1997; Governato et al. 1998; Benson et al. 2001ab). In the more direct simulation technique, the full merging history of each halo in a simulation is stored and the semi-analytic formation prescriptions are implemented on these histories, producing a simulation in which the detailed formation history of each galaxy is followed explicitly (Kauffmann et al. 1999ac; Diaferio et al. 1999 2001; Somerville et al. 2001; Springel et al. 2001; Mathis et al. 2001).

The simulations of Kauffmann et al. (1997) were able to resolve LMC-like galaxies. These authors considered the void probability function (VPF) in an Einstein–de Sitter universe. They computed the VPF for bright ($M_B < -20$) and faint ($M_B < -18$) mock galaxies and for two corresponding random sets of DM particles in the simulation, each chosen to have the same number density as the selected galaxies. While they found in their Figure 14 a similar VPF for bright galaxies and the associated dark matter set, the VPF of their faint galaxies exhibited an extended tail as compared to the DM, showing that these faint objects tend to respect the voids defined by the bright ones, and to segregate from the dark matter.

Kauffmann et al. (1999b, hereafter K99) (see also Benson et al. 2001a) had coarser resolution, and did not compute void statistics. Instead one can get an idea of their predicted voids by means of the pictures of the galaxy distribution they provide. As noted by P01, visual inspection of the simulations shows large regions between the concentrations of L_* galaxies in clusters and filaments, which appear almost empty of galaxies (see figure 5 of K99). However, the extent to which these simulated voids retain a significant fraction of the mass, in the form of LMC-sized or smaller DM haloes, is unclear, even in the low-density Λ CDM model. If there are haloes in the voids, then no galaxies have been associated with them by the galaxy formation algorithm, and one has to check if this is due to the resolution limit or to a well-determined physical process.

If simulations still show a substantial number of lower mass DM haloes in “voids”, P01 considers this observed suppression of galaxy formation a “potential crisis” for the Λ CDM paradigm. Note, however, that there may be possible remedies: for example, ionizing fluxes from the first struc-

tures may suppress nearby dwarf galaxy formation (Rees 1985; Srianand 1997; Cen & Ostriker 2000, see also Friedmann & Piran 2001). Alternatively, the Warm Dark Matter model of Bode et al. (2001) may help to solve the issue.

The goal of this paper is to help to clarify the situation of voids from a *numerical* point of view, using the Λ CDM simulation presented in Mathis et al. (2001, hereafter M01). This simulation was constrained so that the present-day DM distribution mimics the large scale structure of the local universe up to a distance of 8000 km s⁻¹ from the Milky-Way. Galaxy formation was followed in this simulation using techniques similar to those of K99 and mock catalogues were extracted for comparison to the observed nearby galaxy distribution. The main clusters in the simulation appear at the position of observed clusters like Coma, Virgo, Hydra, Perseus and Centaurus and larger scale structures, including voids, correspond well. The simulations can track the formation and morphological evolution of dwarf galaxies of the size of the LMC, and can resolve the luminosity of galaxies 6 times fainter. The corresponding *morphology* and *luminosity* resolution limits of the simulation (defined as the mean, present-day *B*-band luminosities of the central galaxy of a 10 and 100 particle halo respectively) are $M_B = -16.27$ and $M_B = -18.46$. They correspond to halo virial circular velocities of haloes of ~ 54 and ~ 103 km s⁻¹ and masses of $\sim 3 \times 10^{10}$ and $\sim 3 \times 10^{11} h^{-1} M_\odot$ respectively (here and below we take $h=0.7$ when quoting absolute magnitudes).

The morphology resolution of the CR Λ CDM simulation is only a factor 3 better than that of Kauffmann et al. (1997) but the volume simulated is 3 times larger. Also, the Λ CDM model currently seems a better bet than the EdS model they assumed. In addition the current galaxy formation algorithm is based on a much more detailed model including morphological evolution of the galaxies via merging, explosive (bursts) and quiescent star formation, and feedback.

Below we begin by using simple, “one-point” statistics to bring out a hypothetical void population. From the DM skeleton alone, we are able to check the claim of P01 on the fraction and typical masses of the haloes residing in underdense volumes. Simply by visual inspection of the DM distribution, we highlight regions which are depleted of even the smallest haloes that we can follow.

Then, within the whole simulated galaxy population, we select several subsamples (candidates for a void population), splitting according to a variety of possibly relevant properties: luminosity, colour, morphology. Also, we extract sets of haloes, binned by total mass. We study the typical densities (estimated on a 5 h^{-1} Mpc scale) in which these various populations reside, with the goal of finding a first signature of a void population. We recover the well-known pattern of halo bias. Blue, star-forming galaxies tend to reside in underdense regions, a trend which is also present but is not so marked for bulge-less galaxies.

Next we estimate the environment density dependence of the galaxy luminosity function, focussing on the variation of the shape and the normalization of the LF with the local mass density. We compute LFs in a series of density bins covering equal total volumes, and then in bins containing equal total mass. While the overall normalization of the LF is quite different between equal-volume bins, it is very similar between equal-mass bins. We find some tendency for

the faint-end slope of the LF to vary with DM environment density.

Finally, we consider “multi-point” probes like correlation functions and nearest neighbour statistics. The correlation functions of our samples provide a check of the selection procedure. We recover the usual behaviour: in particular, red galaxies are much more clustered than blue ones, in agreement with K99. We stress, however, that it is difficult to deduce the relative spatial distribution of populations on the basis of their correlation functions.

Since Soneira & Peebles (1977), nearest neighbour statistics have been a common observational tool to discriminate between spatial distributions of objects. We carry out such an analysis in real space for our series of subsamples, taking L_* spiral galaxies as the neighbour population (following P01). We find that blue, star-forming galaxies are more weakly associated with L_* spirals than are other L_* spirals but otherwise we find no significant effect. We conclude that there is no dwarf-type void population in the simulation, down to our resolution limit.

The disposition of our paper is as follows: in Section 2, we begin with a qualitative, visual comparison between the galaxies that have formed in a void and in a cluster environment. The distribution of haloes in our void does not support the assertion of P01 that the voids should contain small haloes. Then, in Section 3, we describe the characteristics of our galaxy and DM halo subsamples. We show the distribution of our reference spirals in a slice spanning the supergalactic plane. Section 4 evaluates the environment densities for the various mock samples, and computes the density dependence of LFs. We switch to two-point statistics in Section 5. We check the correlation functions of our subsamples and then carry out a nearest neighbour analysis similar to that of P01. We summarize and conclude in Section 6.

2 AN EXAMPLE OF THE GALAXY DISTRIBUTION IN A “VOID”

Figure 3 of M01 (see also the bottom right panel of Fig. 1 below) plots the simulated galaxy distribution within 8000 km s⁻¹ of the Milky-Way, in a slice of thickness 30 h^{-1} Mpc centred on the supergalactic plane. Two large voids are visible: the first at (-60,-30) h^{-1} Mpc in (SGX,SGY), with a diameter of $\sim 20 h^{-1}$ Mpc, the other nearly opposite to the MW, at (40,50), where a galaxy separates two smaller voids, of diameter $\sim 10 h^{-1}$ Mpc each. The same voids are seen in the real galaxy distribution for example the *PSCz* survey (consider Figure 2 of Plionis & Basilakos 2001).

As an example, we focus here on the void located at (40,50) h^{-1} Mpc, since it lies further inside high resolution region of the simulation, and may be less affected by the transition from the high-resolution to the low-resolution zone. We excise a cubic region of side 24 h^{-1} Mpc centred on the middle of the void.

The top left panel of Fig. 1 shows the distribution of all galaxies within this cube brighter than our luminosity resolution limit. The colors of the symbols scale with the $B - V$ index, and their sizes with the B-magnitude of the galaxies. Because of the galaxy formation scheme adopted in M01, all DM haloes in the simulation with 10 or more

particles contain at least one galaxy. Furthermore, with our definition of the luminosity resolution limit (the mean luminosity of the central galaxy of a 10-particle halo), one expects that a fair fraction of the haloes more massive than $10 \times M_{part} = 3.57 \times 10^{10} h^{-1} M_{\odot}$ will have an associated galaxy with $M_B \leq -16.27$, and so will appear on the top left picture of Fig. 1. In the region shown, 75% of all haloes have a central galaxy at least this bright. This is shown explicitly in the bottom left panel of Fig. 1, where we project the same low density region as in the top left panel, and mark with circles the positions of all DM haloes with 10 or more particles.

There are two obvious voids completely depleted of haloes, with diameters of order 10 and 8 h^{-1} Mpc and depths of 24 h^{-1} Mpc. This contradicts P01 who claims that in a Λ CDM model, low mass haloes should spread fairly evenly through the voids defined by the larger ones. In fact, gravity seems to have moved them out of these voids.

For comparison, we give in the top right panel of Fig. 1 the galaxy distribution around the simulated Virgo cluster ($M_{200} \sim 4 \times 10^{14} h^{-1} M_{\odot}$), also plotted in a cubic region of side 24 h^{-1} Mpc centred on the cluster centre. The galaxy symbols follow the same rules and scales as in the left panel. Note that to avoid saturating the cluster region, galaxies are plotted down to $M_B = -17$ only.

3 DEFINING MOCK GALAXY SAMPLES

The few isolated galaxies observed in the Bo tes void are normal, late-type spirals (Szomoru et al. 1996ab). Nevertheless, there is a widespread belief that voids should be filled by late-type and low surface brightness dwarfs. Observational programs have targetted a number of different potential “void” populations: Eder et al. (1989) and Lee et al. (2000) considered dwarf galaxies; Pustil’nik et al. (1995) and Lindner et al. (1996) looked at blue compact galaxies (BCG); Salzer et al. (1990) separated their sample between high and low luminosity galaxies (with a limit at $M_B = -18$), and Bothun et al. (1993) looked for low surface brightness galaxies (LSB). In his unsuccessful quest for a possible void population in the *ORS*, P01 considered dwarfs/irregulars and LSBs, computing the distribution of distance from these objects to their nearest neighbour L_* spiral.

To evaluate how biases arise in our simulations we will first study the environments of dark haloes as a function of their mass, and evaluate how their well-known clustering bias (e.g. Mo & White 1996) is echoed in the statistics that we later apply to our galaxy populations.

Then, using the photometric and morphological information provided by the simulation, we study galaxy environments as a function of luminosity, morphology, and colour. For example, we will compare the environments of faint galaxies to those of bright ones. To make contact with P01, we also analyze the nearest neighbour statistics of our various halo and galaxy samples by looking for the nearest neighbour of each test object among a set of reference L_* spirals.

Figure 1. Top left: the present-day distribution of all galaxies brighter than the resolution limit ($M_B < -16.27$) in the void region defined in Section 2 and selected from the Λ CDM simulation of M01. The region shown is cubical and has a side of $24 h^{-1}$ Mpc. The size of the symbols scales with the B -band luminosity of the galaxies and their colour with the $B - V$ index. Top right: the present-day distribution of galaxies in a region surrounding the “Virgo cluster” in this same simulation. Galaxies are restricted to $M_B < -17$ (to avoid saturating the cluster region), colour and size of the circles scale as previously. Bottom left: the halo distribution in the same region as in the top left picture. The same two voids as in galaxy distribution are apparent. Bottom right: the standard or “reference” late-type galaxies in the whole simulation, in a slice $30 h^{-1}$ Mpc thick in the SGZ direction encompassing the SG plane. The side of the picture is $180 h^{-1}$ Mpc long. Colour and size of the symbols follow the previous rule. A high resolution copy of this Figure can be found at <http://www.mpa-garching.mpg.de/NumCos/CR/Voids/>

3.1 Reference galaxies

These galaxies will be used as standard objects defining the clustering of “typical” galaxies, in particular for our nearest neighbour statistics. We select bright spirals within one magnitude of $M_{B,*} \sim -20.8$ (taken here as the typical magnitude of a Milky Way look-alike): $-21.8 \lesssim M_B \lesssim -19.8$, and with Sa/Sb/Sc morphological type: $1 < M_{B,\text{bulge}} - M_{B,\text{total}} < 2.2$ (Simien & de Vaucouleurs 1986; de Vaucouleurs et al. 1991). This criterion is similar to the one used in the construction of the Tully-Fisher relations in M01, but includes Sa galaxies as well. We do *not* require that these reference galaxies be the central galaxies of their haloes however: they may also be satellites orbiting in large clusters. We found 1471 such galaxies in the whole simulation, an abundance very close ($7 \times 10^{-4} h^3 \text{Mpc}^{-3}$) to the value used by P01 for the spiral galaxies in his analysis of the distribution of a population of LSB galaxies at distances $6000 \leq cz \leq 9000 \text{ km s}^{-1}$.

The bottom right panel of Fig. 1 shows these reference galaxies in a slice of side-length $180 h^{-1}$ Mpc encompassing the supergalactic plane. Even with our applied morphological criterion, although the *rms* spread in the colors of the reference galaxies is small, there are still some red galaxies. This is not unexpected, however; most of these objects are “anemic” spirals in clusters. In the following, we will refer to this sample of reference galaxies as *Ref*.

3.2 DM haloes

We construct a series of dark matter halo samples binned according to their total mass (taken here to be the number of particles linked by the *FOF* algorithm). We define our mass bins to span a factor 4, with the “smallest bin” having [10 40] particles per halo and the largest [40960 163840] particles (there are only 38 haloes in this last bin, and only 5 haloes with more than 163840 particles). We call the 7 resulting samples HM_1 to HM_7 (Halo Mass) from the lightest to the heaviest. The *lower* limits (in particle number and mass) for each of the 7 bins are given in the first 7 columns of the first two lines of Table 1, while the last column gives the *upper* limit of the most massive bin, HM_7 . The third line gives the number of haloes in each bin.

3.3 Luminosity selection

We define a series of luminosity bins to bring out the trends in the spatial distribution of objects as one goes from bright

galaxies down to dwarfs. Our most luminous bin (which contains only 29 galaxies) has $M_B < -22.5$ and subsequent bins span one magnitude to a lower limit of $M_B = -16.5$, close to the resolution limit. This results in 7 bins labelled GL_1 to GL_7 (Galaxy Luminosity) from the faintest to the brightest. The limits of the luminosity bins, and corresponding number of objects, are given in the fourth and fifth lines of Table 1.

3.4 Colour selection

From figure 7 of M01, we can infer that $B - V \sim 0.8$ splits galaxies brighter than the morphological resolution roughly into ellipticals and spirals. However, this split is not perfect, as noted above for the reference galaxies. Moreover, since we want to highlight a progressive change in the spatial distribution of galaxies with a given property, we will proceed as in the previous paragraph. We split the range covered by the $B - V$ index of all galaxies above the luminosity resolution limit of the simulation ($0 \lesssim B - V \lesssim 1.42^\dagger$) in a series of 7 bins called GC_1 to GC_7 (Galaxy Colour), from the bluest to the reddest. The bluest bin is [0 0.5], and the following bin thresholds are separated by 0.1 in $B - V$. The last bin covers the range [1 1.5]. Again, the limits of the bins, and number of objects, are given in the sixth and seventh lines of Table 1.

We stress that we have binned up all galaxies above the luminosity resolution limit of our simulation. This allows us to go substantially fainter than if we restricted ourselves to galaxies for which the simulation gives reliable morphologies.

3.5 Morphology selection

Our last sample selection makes use of the morphological information in the simulation. By definition, we need here to restrict ourselves to the galaxies brighter than the morphology resolution limit ($M_B \leq -18.46$). The sample selection is done according to $M_{B,\text{bulge}} - M_{B,\text{total}}$ (which ranges from 0 to ~ 7 among the simulated galaxies which possess a bulge). The bins are called GM_1 to GM_7 (Galaxy Morphology) from the least bulge-dominated to the most bulge-dominated. Note that for simplicity, we have put bulge-less

[†] $B - V \sim 1.4$ is the maximum reached in our simulation: although stars are assumed to always form with solar metallicity and a Scalo IMF, the approximate model for dust reddening that we subsequently apply to the mock galaxy catalogs yields a few galaxies that are very red

Table 1. The *lower limits* of the bins used to define the halo and galaxy samples. The last column gives the *upper limit* of the 7th bin. The first three rows are for the dark matter haloes binned by mass, the following pairs of rows are for the galaxies split by luminosity (M_B), colour ($B - V$), and morphology ($M_{B,\text{bulge}} - M_{B,\text{total}}$), respectively.

Property	1	2	3	4	5	6	7	Upper limit
Halo particle number	10	40	160	640	2560	10240	40960	163840
Halo mass (M_\odot)	5.1×10^{10}	2.0×10^{11}	8.2×10^{11}	3.3×10^{12}	1.3×10^{13}	5.2×10^{13}	2.1×10^{14}	8.4×10^{14}
Number of objects	183552	40871	11243	2948	861	214	38	
Galaxy luminosity (M_B)	-16.5	-17.5	-18.5	-19.5	-20.5	-21.5	-22.5	$-\infty$
Number of objects	120261	46473	17961	7103	2876	446	29	
Galaxy colour ($B - V$)	0	0.5	0.6	0.7	0.8	0.9	1.0	1.5
Number of objects	16141	32801	78908	36193	12634	34759	8434	
Galaxy morphology	∞	4	2	1	0.75	0.5	0.25	0
Number of objects	4255	7004	8219	3093	3410	1688	1748	

galaxies (above the morphology resolution) together with the objects in the first bin. The last two lines of Table 1 give the limits of these ‘‘morphology’’ bins, together with the associated number of objects.

4 THE ENVIRONMENTS OF THE GALAXY POPULATIONS

To compare the local environments of the various samples, and to look for a possible simple signature of a void population, we first compute the mass density (by smoothing the DM field) of the region surrounding each galaxy, and we compare the distributions of this local density in our various samples. In addition, we estimate the luminosity function (per unit mass) of objects lying in environments of given density, focussing particularly on the variation of the overall shape.

4.1 Density of the environments

4.1.1 Method

We characterize the environments of the galaxies by mass densities smoothed over a $5 h^{-1}$ Mpc smoothing scale (a smoothing of $10 h^{-1}$ Mpc is already too large to bring out any trends between the samples).

We assign the DM distribution of the simulation on a fine regular grid with mesh spacing much smaller than one smoothing length (R_s), using a CIC scheme. The smoothing of the density field is performed on this fine grid by means of a Gaussian kernel which takes the form:

$$W(r) = \frac{1}{(2\pi R_s^2)^{3/2}} \exp\left(\frac{-r^2}{2R_s^2}\right) \quad (1)$$

where we take $R_s = 5 h^{-1}$ Mpc. Because we expect to study preferentially large voids with a diameter of $\sim 10 h^{-1}$ Mpc, this scale seems appropriate.

Note that because we have only followed galaxy formation in the central, roughly spherical, high-resolution region

of simulation (with radius $\sim 8000 \text{ km s}^{-1}$), we also use a shell of low-resolution particles immediately beyond to get the correct estimate of the DM density at mesh points near the boundary. Once we have sampled the smoothed DM field, we then simply interpolate the overdensities computed on the grid to the positions of the DM haloes (given by their most bound particle) or of the galaxies.

We consider then the normalized cumulative counts of the number of galaxies (the population fraction) above a given mass overdensity threshold, as a function of decreasing overdensity, starting from $\delta_s \gtrsim 30$ the maximum we find for the $5 h^{-1}$ Mpc smoothing length we use. If the galaxies of some test population reside preferentially in low-density environments, this will appear as a late rise of the cumulative fraction with decreasing DM overdensity, compared, for instance, to the behaviour of the reference galaxies.

By construction, the cumulative plots obtained from the galaxy positions are mass- rather than volume-weighted. The visual impression from the pictures of K99 recalled by P01 is one of very few simulated galaxies in the voids, with the latter filling a substantial fraction of space. A simple way to assess the departure of the distribution of galaxies from a homogenous one with the tools of this Section is to use the regular mesh from which we have interpolated the DM density to the galaxy positions. In the four plots of Fig 2, the repeated dotted line gives the cumulative fraction of mesh points above a given smoothed DM overdensity threshold: it should be viewed as the simulation volume fraction above the threshold. We will denote this ‘‘mesh sample’’ with V , and note that half of the simulation volume has a DM environment density of δ_s below -0.24 and only about a third of it has higher than average density.

In the same four plots, we also repeat the cumulative fraction of the reference galaxies with a solid line. This line is very close to that we find for the DM particles themselves (thus for the ‘‘mass’’ in the simulation) and is a translation by almost a factor 2 towards higher density from the V cumulative fraction: each population fraction is reached in

the *Ref* sample at twice the DM density needed to reach the same fraction for the uniformly distributed *V* population.

4.1.2 Results for mass and luminosity splitting

In the top left panel of Fig. 2 we show with dashed lines the normalized cumulative counts of the halo samples selected by mass (HM_i). In each of the four plots of Fig. 2 that we discuss here, the lowest and highest sample indices ($i = 1$ and $i = 7$) correspond to the leftmost and rightmost dashed curves, respectively, with a monotonic variation for the samples in between.

The first three halo samples HM_1 to HM_3 contain haloes with total masses $M_{\text{tot}} \lesssim M_*$, where as usual we define M_* such that $\sigma(M_*) = \delta_{\text{crit}} \sim 1.69$ ($M_* \sim 1.44 \times 10^{13} M_\odot$ here). The behaviours of the fractions of cumulative counts for these three halo samples are very similar: at overdensities under $\delta_s \sim 0.6$ they depart slightly from the counts of the *Ref* sample, favoring lower density environments. However, the plots are still far from the cumulative fraction for the grid counts; the population of haloes is 90% complete for $\delta_s \geq -0.3$, while a third of the simulation volume is at such low densities.

While the plot of HM_4 almost coincides with the *Ref* cumulative fraction (88% of the *Ref* galaxies are central galaxies of haloes, and 53% of them are central galaxies of HM_4 haloes), the three most massive halo bins separate strongly from each other and from the *Ref* fraction. This is a clear effect of the non-linearity of halo bias: according to the model of Mo & White (1996), one writes:

$$b_{\text{halos}}(\nu) = 1 + \frac{\nu^2 - 1}{\delta_{\text{crit}}}, \quad (2)$$

where $\nu = \delta_{\text{crit}}/\sigma(M)$. Haloes less massive than M_* are anti-biased, haloes close to M_* like HM_4 are unbiased, and the bias becomes more and more substantial as one further increases the mass. Haloes of the most massive sample completely avoid low and mean density regions (recall also that the particles of a given halo contribute to the smoothed DM density estimation of the region it resides in). In particular, there are no haloes in the HM_7 sample lying in environments with $\delta_s \leq 1.5$.

The top right panel of Fig. 2 shows the cumulative fraction of the galaxy samples binned by their luminosity (GL_i). The trends are similar to those of the halo samples selected by their total DM mass, but except for the most luminous sample, the range of variation of galaxy bias is much reduced. Of course this is due to the fact that there is no tight relation between a halo mass and the luminosity of its central galaxy, and that a given galaxy luminosity sample has contributions from several differing halo samples. An example of this dilution is the cumulative fraction of the counts of the first four galaxy samples, which are very similar, and are very close to the *Ref* sample. The range of *B*-band luminosities of the *Ref* sample encompasses those of the GL_4 and GL_5 samples together. The further match with the GL_1 to GL_3 samples shows that the population of faint galaxies (i.e. taken globally in the samples and selected solely by luminosity) does not constitute a void population. GL_4 and GL_5 galaxies increasingly tend to avoid underdense regions ($\delta_s \leq 0$) where a few *Ref* galaxies are found. The most luminous bin, GL_7 , with only 29 galaxies, contains of course a

fair fraction of galaxies in very dense environments (BCGs in regions with $\delta_s \sim 10$). However, as compared to HM_7 , there are also very bright galaxies in the *B*-band in mean density regions: these are galaxies which have undergone a recent merger and are currently starbursting: among the 7 galaxies of the GL_7 sample with $\delta_s \leq 0.5$, 5 have a colour index $B - V \leq 0.5$ and $M_B \sim -23$. Again, this underlines the difficulty in relating halo mass to central galaxy luminosity.

Recall that the small amount of (anti-)bias found when considering faint luminosities or galaxies close to L_* and the rather limited positive bias for galaxies somewhat brighter (when not extremely bright, though) is consistent with that found in the figure 14 of K99 and with the correlation functions given below.

4.1.3 Results for colour and morphology splitting

The bottom left panel of Fig. 2 plots the fraction of galaxies as a function of environment density among the colour samples (GC_i). Again, the different samples are differently biased with respect to the *Ref* sample. Note, however, that a fair fraction of the galaxies in the two bluest samples populate regions more underdense than any of the other galaxy samples considered here: the curves of GC_1 and GC_2 are close to each other and rise later than that of the *Ref* sample (the HM_1 halo sample also “favours” such underdense regions as compared to the usual trends). 10% of the *Ref* population lies in environments with densities $\delta_s \leq -0.37$ while 10% of the GC_1 population lies at $\delta_s \leq -0.5$. Of course, this is still substantially denser than the corresponding density threshold for the *V* sample: such blue galaxies do not make a homogeneous galaxy population on their own, but they nevertheless constitute the most promising “void fillers”. For increasingly redder populations, a preference for denser environments develops, but even in the reddest sample, there is a small fraction of the population in underdense regions, quite similarly to the GL_7 sample. The fraction of the reddest galaxies in very dense regions ($\delta_s \sim 10$) is of order of 15% and smaller than the 30% fraction for the GL_7 sample (recall also that there are 8434 galaxies in GC_7 , and only 29 in GL_7). Leaving aside GL_7 , one concludes that the variation of bias is stronger among colour selected samples than among luminosity selected samples.

The bottom right plot of Fig. 2 deals with our morphology selected populations (GM_i). The five samples with later type galaxies show plots of cumulative fractions quite close to those of the reference spirals. Bias with respect to the *Ref* sample, favouring denser galaxy environment, is visible for the two bulge dominated samples. Yet, the preference towards higher densities for extreme GM_7 galaxies is weaker than in our other extreme samples.

To conclude, none of our GM_i populations has galaxies filling low density regions. Note that the morphology–density relation that we have implicitly constructed is limited to objects with luminosities above the morphology resolution at $M_B \sim -18.5$. This might partly explain why we found the GC_1 galaxies (down to the luminosity resolution) to reside on average in lower density regions than the GM_1 galaxies. Low mass haloes with less than 100 particles are generally not expected to host galaxies with $M_B \lesssim -18.5$, simply because they are not massive enough. Then, one can easily understand why any sample constructed by splitting

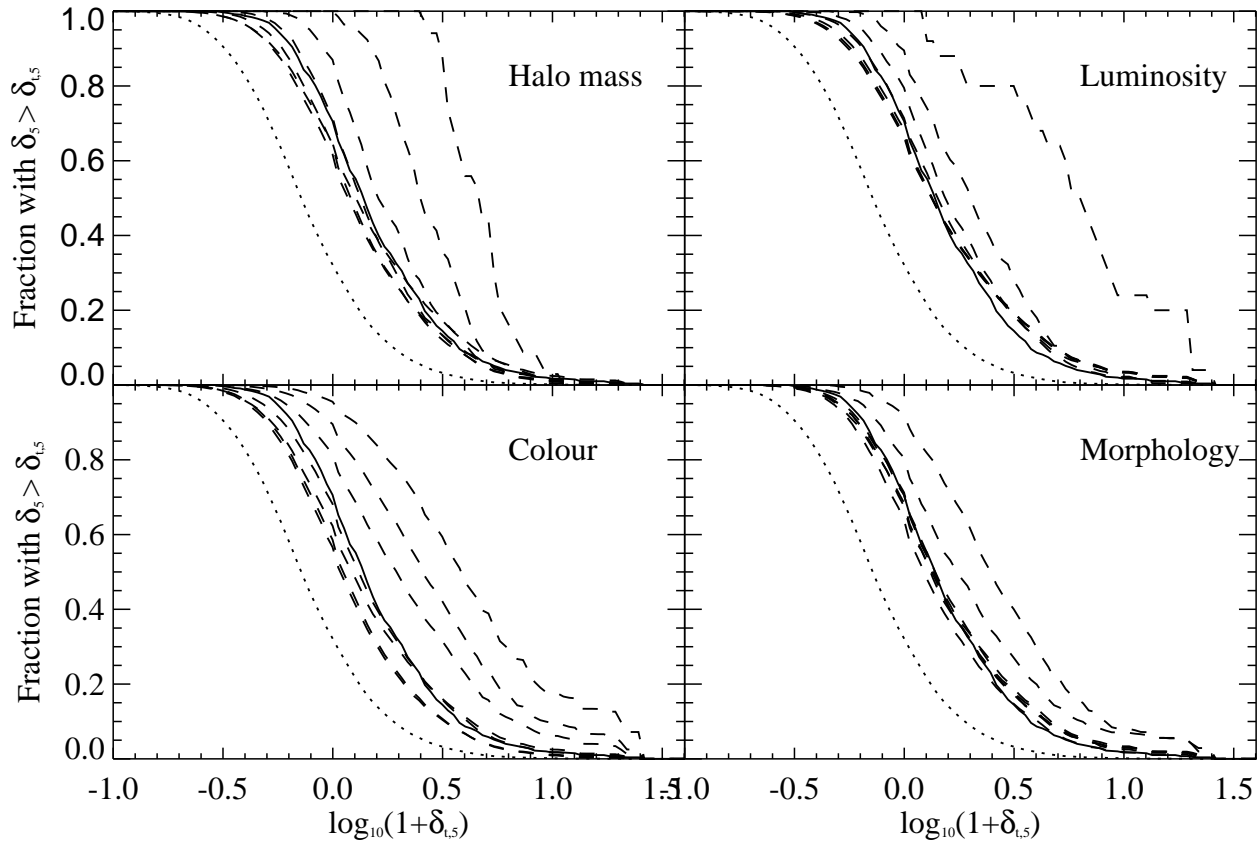


Figure 2. The cumulative fraction of haloes and galaxies as a function of their DM environment density smoothed over $5h^{-1}$ Mpc. In each plot, the dashed lines give the cumulative fraction of the objects in each of the samples (with index 1 and 7 associated to the leftmost and rightmost curves respectively and monotonic index increase in between). The repeated solid and dotted lines give the cumulative counts for the *Ref* (reference spiral galaxies) and the *V* (regular mesh points) samples, respectively. The top left panel is for the DM haloes split by mass (HM_i), the top right panel for galaxies beyond the luminosity resolution limit, split by luminosity (GL_i), and the bottom left and right panels give the cumulative fraction for galaxies split by their colour (beyond the luminosity resolution limit) and by their morphology (beyond the morphology resolution limit), respectively.

the $M_B < -18.5$ galaxy population will not show a curve of cumulative counts below that say, of the HM_3 halo sample.

4.2 Luminosity functions

The previous section has shown that the typical environment (when smoothed on a $5h^{-1}$ Mpc scale) of the galaxies varies only slowly with their luminosities. Conversely, one can look for the distribution of galaxy luminosities as a function of the surrounding DM overdensity. Because a given Eulerian volume corresponds to different mean DM densities and different mean number of galaxies, when we probe different environments, we split our discussion of the luminosity functions (LF) in two series of five adjacent DM environment density bins. The first series (called LFV_i) is set so as to have the same simulation *volume* in each bin (hence probing 20% of the whole volume), and the second one (called LFM_i) to have the same *mass* in each bin (20% of the whole mass). In each of the two cases, we will express the luminosity function in units of counts per magnitude. Obviously with the appropriate *same* vertical shift of all LFs of the LFV_i sample, we could get units of counts per

magnitude per unit volume, and with another *same* shift for all LFs of the LFM_i sample, we could get units of counts per magnitude per unit DM mass. In the first line of Table 2 we give the five lower limits for the DM environment density bins (the upper limit of the last bin is left open), for the LFV_i and LFM_i samples (left and right columns respectively). In the second and third lines of the table, we give the corresponding minimum *B*-band magnitude in each bin, and the number of contributing galaxies.

Here, we are mostly interested in the variation of the shape and normalization of the luminosity function with environment. For instance, if faint dwarf galaxies are to avoid high-density regions and to populate preferentially the voids (for a given enclosed DM mass), one would expect a steeper slope in lower density regions. The environments are again characterized by the DM overdensity smoothed with a gaussian kernel of dispersion $5h^{-1}$ Mpc.

The left and right panels of Fig. 3 give the series of *B*-band LFs, for the LFV_i and LFM_i samples respectively. The tags at the bright ends of the functions label the id's of the different environments (first line of Table 2). The coding of the lines has been alternated for clarity.

Table 2. Minimum smoothed DM density thresholds (δ_s) defining the bins where the LFV_i (left column) and LFM_i (right column) luminosity functions are computed. The second line gives the minimum B -band magnitude among galaxies in each interval, and the third line the number of contributing galaxies.

	Equal volume (LFV_i)					Equal mass (LFM_i)				
Bin number	1	2	3	4	5	1	2	3	4	5
Minimum density	-1	-0.57	-0.38	-0.14	0.33	-1	-0.23	0.23	1	2.6
Minimum B -band magnitude	-20.9	-21.5	-23.1	-23.1	-23.6	-23.1	-23.1	-23.0	-23.8	-23.6
Number of galaxies	5215	13179	20761	33059	89242	32068	34025	34940	29723	30700

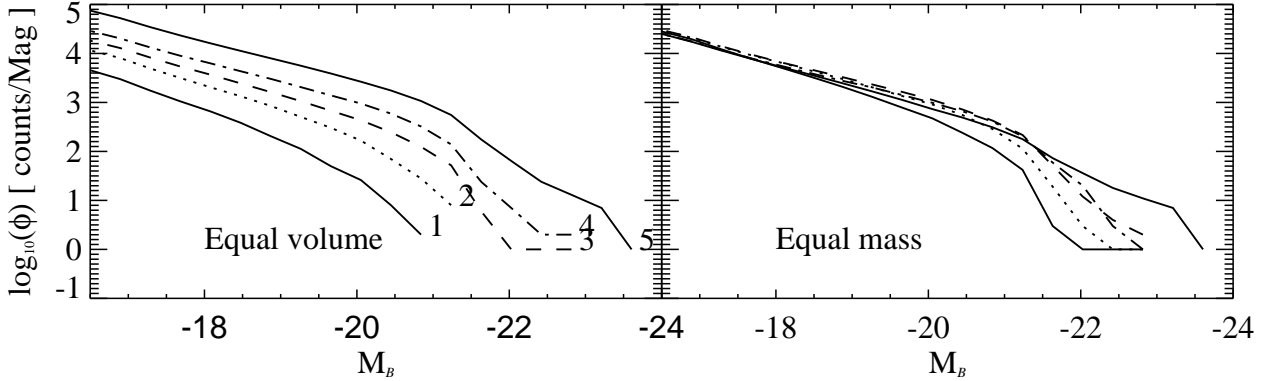


Figure 3. The B -band luminosity functions (in units of galaxy counts per magnitude) for the 5 LFV_i and LFM_i bins (left and right panels respectively). Each of the LFV_i and LFM_i bins covers respectively the same 20% simulation volume and contains the same 20% of the total simulation DM mass. The tags at the bright ends of the LFs in the left panel refer to the bin indices as given by the first line of Table 2. The coding of the lines has no special meaning, but alternates for clarity. It is the same in both panels.

These LFs call for several comments, dealing successively with the minimum magnitude reached by the selected galaxies, the normalisation of the overall LF, the exponential cutoff and the faint-end slope.

- The left panel of Fig. 3 shows how LFs computed for two most underdense bins in the LFV_i sample do not reach as high luminosities as the LFs computed for higher density bins. The second line of Table 2 gives the minimum B -band magnitude of the galaxies in each bin. While they hardly reach $M_B \sim -21$ and $M_B \sim -21.5$ for $\delta_s \lesssim -0.57$ and -0.38 respectively, there are already bright galaxies with B -band luminosities characteristic of the BCGs of massive clusters ($M_B \sim -23$) in the third and fourth bins with $-0.38 \leq \delta_s \leq 0.33$, probing volumes with DM densities close to the mean. These brightest objects are typically undergoing a starburst associated with a major merger, which brighten up in the B -band. Recall that our adopted TF normalization means that, on average, a central spiral galaxy of a halo with $V_{200} \sim 220 \text{ km s}^{-1}$ has $M_B \sim -20.8$. Of course, the last sample LFV_5 contains the BCGs of the most massive clusters, and as expected we find there the brightest galaxy ($M_B \sim -23.6$) of the whole simulation. The first four LFs of the LFM_i bins given in the right panel of Fig. 3 have comparable maximum galaxy luminosities. The absence of segregation from the point of view of the luminosity of the brightest galaxies among the bins of this sample is only due

to the modified density thresholds of LFM_i compared to those of LFV_i : already LFM_1 probes smooth DM densities reaching high enough to include the starbursting galaxies mentioned above.

- Although the low density regions covered by LFV_1 constitute 20% of the simulation volume, they only contain 4% of the total mass. At the other extreme, the LFV_5 bin carries 57% of the total mass in quantitatively the same volume and naturally hosts a larger number of galaxies. This readily explains the difference in the overall normalization (counts of galaxies) of the LFs in the LFV_i samples, as one goes from low density regions to high density ones. As expected, the LFs in the LFM_i sample have quite similar normalizations (at $M_B \sim -17$): each bin contains a similar mass. Interestingly, even the first bin which is restricted to $\delta_s \leq -0.23$ and which encompasses 55% of the simulation volume does not host a very different number of faint (say with $-16.5 > M_B > -17.5$) galaxies per DM mass than does, e.g. LFM_3 which covers 13% of the volume. This argues against a strong luminosity–density relation at the faint end (at the simulation resolution) and seems to confirm that the faint galaxy population does not predominantly reside in voids.

- An “exponential” cutoff is visible for the samples LFV_3 and LFV_4 probing mean density environments. It is weaker for LFV_1 and LFV_2 , simply because in “void” and under-

dense regions, the LFs do not reach bright enough luminosities where one would expect the cutoff. The most overdense sample LFV_5 shows a complicated behaviour, one can notice a possible cutoff at $M_B \sim -21$, beyond which the LF exhibits sort of an “inflexion point” at $M_B \sim -21.5$ or -22 . This presumably echoes the difficulties encountered by M01 in obtaining good-looking cluster luminosity functions at the bright end. Again due to the shift in maximum density thresholds towards higher densities for all LFM_i bins compared to the LFV_i sample, cutoffs at $M_B \sim -21$ make a clear feature of the first four samples of LFM_i . It is reassuring for the galaxy formation scheme that these “knees” break the LFs at very similar magnitudes. Again, the presence of a cutoff for LFM_5 is less obvious because of the rather uncertain modelling of the luminosity of the BCGs of massive clusters.

- Faint-end slope variation is visible in both samples, and is more striking in the case of LFM_i . Over the range $[-16.5, -19.5]$, a rough estimation is $\alpha \sim -1.6$ and $\alpha \sim -1.4$ in the lowest and the highest density bins respectively. These estimations repeat for LFV_i . This steepening in the faint-end slope in underdense regions is due to the relative depletion of L_* galaxies in such environments when compared to mean density or overdense environments, while the counts of faint galaxies with $M_B \sim -17$ are similar in the two cases.

The above results assume that at the lowest luminosities considered, no major physical process has been neglected. In particular, the extrapolation to even fainter luminosities of the model for galaxy formation that has been used here is hazardous: for example, background UV radiation (Thoul & Weinberg 1996) must be included when computing the infall rate of the cold gas on haloes with small mass ($V_{200} \sim 30 - 50 \text{ km s}^{-1}$), which collapse late, after reionization. Similarly, reheating by SNe feedback could very well expell a large fraction of the cold gas from the smallest haloes and suppress subsequent star formation there. Note also, as discussed at length in M01, that the overall luminosity function of the model analyzed here is a relatively poor fit to that observed. The results of this Section should thus be taken as indicating the expected trends in cutoff luminosities and faint-end slopes rather than their specific values.

5 CLUSTERING OF THE GALAXY POPULATIONS

In this Section, we consider “two-point” statistics: first we check the correlation functions (in real space) of our samples. We recover the usual results, and underline the particularly low clustering of the “blue” sample with respect to the underlying DM, the latter being at the level of the reference spiral population. We then use nearest neighbour statistics to gain better insight into the relative spatial distribution of the reference galaxies and the various test populations.

5.1 Correlation functions

In both panels of Fig. 4, we reproduce the real-space autocorrelation functions of the DM (upper solid line), together with the autocorrelation functions of our reference galaxies (dash-dotted line). In the left panel, we show the correlations

of the HM_1 and HM_5 samples (dotted lines, with HM_1 having the lowest amplitude on large scales), and the correlations of the GL_1 and GL_5 samples (dashed lines, with GL_1 having the lowest amplitude on large scales). In the right panel, we give the correlations of the GC_1 and GC_7 samples (dotted lines, with GC_1 below the solid line) and the correlations of the GM_1 and GM_7 samples (dashed lines, with GM_1 below the solid line). Note that we show the correlations of HM_5 and GL_5 instead of HM_7 and GL_7 simply because of the small number of objects in these last two samples, which results in too noisy correlation functions. The straight solid line in the lower left corner of each panel shows a -1.8 slope. All correlation functions have been computed from $500 h^{-1} \text{ kpc}$ to $20 h^{-1} \text{ Mpc}$. When interpreting these plots it is important to remember that the region simulated is quite small and is constrained to match the large-scale structure of the observed nearby galaxy distribution. As M01 show, the model autocorrelation functions of the various galaxy populations agree well with the observed functions for galaxies in the corresponding volume.

The logarithmic slope γ of the autocorrelation of the dark matter is close to -1.8 . In the left panel, all samples, including *Ref*, have a shallower slope, closer to -1.4 . This value is also close to the slopes of both the GC_1 and GM_1 samples in the right panel. The other extreme samples, GC_7 and GM_7 , have steeper correlation functions. The curves differ most noticeably, however, in amplitude (bias), even on large scales ($\sim 20 h^{-1} \text{ Mpc}$). Note that the steeper slope of GC_7 compared to, e.g., GC_1 is a consequence of the colour bias being stronger at smaller scales, as is evident in the observational sample of Willmer et al. (1998).

In the left panel of Fig. 4, it is striking how the autocorrelation of HM_1 matches that of the reference spirals, on scales greater than $\sim 2 h^{-1} \text{ Mpc}$. The autocorrelation of GL_1 also approaches the correlation of the *Ref* sample on these scales, but it is somewhat stronger. On smaller scales, the GL_1 sample is more correlated than both HM_1 and *Ref*. On the other hand, the autocorrelations of GL_5 and HM_5 are very similar on all scales shown. The reason might be that 88% of the galaxies of the GL_5 are central galaxies of haloes, and 82% of them belong to HM_4 or HM_5 haloes.

Note that the bias between GL_1 and GL_5 is apparent on scales greater than $4 h^{-1} \text{ Mpc}$, beyond which it stays constant at a level of 1.2 to 1.3. A similar behaviour for the halo bias is seen between HM_1 and HM_5 . Such a low level of respective bias is surprising given the rather different masses in the two samples: from equation 2, one would expect $b_1 = 0.53$ and $b_5 = 1.14$ and so $b_{51} = 2.15$, using the mean masses of the haloes in each sample, but note that the more accurate formula of Jing (1998) predicts somewhat smaller effects in the sub- M_* range ($b_{51} \sim 1.7$). We have also already seen that the moderate amount of galaxy bias does not contradict the one given in the top left plot of figure 14 of K99 (although for brighter galaxies).

Finally, the correlation of the reference galaxies is notably antibiased with respect to the DM on small scales ($\lesssim 3 h^{-1} \text{ Mpc}$). On larger scales, the antibias reaches an almost constant value of 1.2. Again, this antibias of the late-type, star-forming galaxies was also noticed by K99.

As shown in the right panel of Fig. 4, the bias between GC_1 and GC_7 and between GM_1 and GM_7 is much stronger than between GL_1 and GL_5 for instance. As for the left-

hand plot, the correlation functions of the first samples GC_1 and GM_1 match very well the autocorrelation of the reference galaxies. We therefore stress that the correlation of the bluest galaxies is *not* much weaker than that of the reference spirals. The correlation of the elliptical galaxies (GM_7) parallels that of the DM with a strong constant bias of ~ 1.6 with respect to the matter. Consistently with the analysis of K99, the colour bias is even higher than the morphology bias, but varies significantly with scale, from $b \gtrsim 3$ on small scales of order $2 h^{-1}$ Mpc, until it reaches the smaller bias of the elliptical galaxies at $15 h^{-1}$ Mpc. This can be explained by the contribution of faint, very red, satellite galaxies in massive haloes which increases the correlation function on small scales, while the morphology luminosity limit applied in the elliptical sample GM_7 suppresses such contribution.

This discussion of autocorrelation functions should be viewed as a mere check that we recover the usual trends among the samples. As stressed by P01, it is not possible to infer the relative spatial distribution of the populations on the basis of their correlation functions alone.

5.2 Nearest Neighbour Statistics

5.2.1 Method

The nearest neighbour analysis compares the cumulative distribution of the distances D_{to} to the nearest “ordinary” neighbour from galaxies in a test sample (for example, irregulars) to the cumulative distribution of the distances D_{oo} from an ordinary galaxy to the nearest other ordinary galaxy. If an extended tail appears in the distribution of D_{to} compared to D_{oo} , the spatial distributions of ordinary and test galaxies differ. In this case, if ordinary galaxies define large voids, test galaxies will tend to populate them. The reader is redirected to P01 for more details.

Here, given the number density of the galaxies in our samples and the probable maximum radius of the voids in the simulation, we expect that both the maximum distance of a t-galaxy to its nearest o-galaxy and the maximum distance of an o-galaxy to its nearest o-galaxy will be of order $15 h^{-1}$ Mpc. As a result, we limit the centers (t and o) to the innermost $65 h^{-1}$ Mpc around the MW (the high-resolution zone of the simulation has a radius of $\sim 80 h^{-1}$ Mpc). To avoid possible complications due to peculiar velocities of galaxies, we compute nearest neighbour statistics in real space. Although P01 carries out his whole analysis in redshift space, we have checked that the induced difference is negligible for the points we want to make.

To assess the significance of our results (and again following P01), we also randomize in the whole simulation volume the positions of one third of the galaxies in each test sample, and recompute D_{to} . This shows the effect of having at least *one third* of the test population *homogeneously* distributed. In the following, we consider this level as our lower “detection” limit for finding a void population. This procedure is clearly somewhat arbitrary but allows direct comparison with P01.

5.2.2 Results

Fig. 5 gives the nearest neighbour statistics for each of our four sets of samples (see labels). In each case, the cumula-

tive fraction of the distance from a reference galaxy to its nearest reference galaxy (D_{oo}) is shown by the solid line (the same in all the plots in this Section). The cumulative fraction of the distance from a test galaxy of the various samples to its nearest reference galaxy (D_{to}) is given by the dashed lines. In all cases, the rightmost dashed curve corresponds to index 1 of the samples, the leftmost dashed curve to index 7, and the indices increase monotonically in between. To show the level of a homogeneous population, we spanned the innermost $65 h^{-1}$ Mpc of the simulation with a regular mesh with cell size $5 h^{-1}$ Mpc, resulting in ~ 10000 points. We chose this size to end up with approximately the same density as in our bluest sample of galaxies, GC_1 . The cumulative fraction of such mesh points as a function of the distance to their nearest spiral neighbour is repeated with dots in the four panels of the Figure.

The Fig. 6 shows the cumulative fractions D_{to} for the extreme bins (1 and 7) (as an exception, HM_6 in the right panel for reasons of noise) of each of our population samples, as computed initially (dashed lines) and after randomizing the positions of one third of the test galaxies through the whole simulation volume (dash-dotted lines). The cumulative fraction of the mesh points as a function of the distance to their nearest spiral neighbour is also shown with dots. Note, as expected, that we found the curves of the randomized objects of the intermediate samples always to lie between those of the randomized objects of the extreme samples, and so we do not plot them.

The signature of halo bias is well visible. The haloes of the least massive sample, HM_1 , have farther nearest spiral galaxies than do the spiral galaxies themselves ($D_{to} > D_{oo}$): the rightmost dashed curve lies well above the solid curve. This holds for the next two samples too, but to a lesser extent. Hence, these small haloes are more broadly distributed than the reference spirals. The overall agreement of D_{to} with D_{oo} for HM_4 and for HM_5 ($M_{200} \sim M_*$) can be understood in the same way as in Fig. 2.

At separations greater than $\sim 4 h^{-1}$ Mpc, the two most massive halo samples have nearest spiral neighbours which are on average much closer than those of the *Ref* galaxies. Of course, such massive haloes are found almost exclusively in dense environments with more galaxies, and can also be in the process of accreting spirals from the field. Also recall that it is possible for haloes to find their nearest neighbour among their own galaxy population.

Only a fraction of the least massive haloes *could* be homogeneously distributed with respect to the spirals, but in the top left panel of Fig. 6, the dash-dotted line of the cumulative fraction of D_{to} for the HM_1 sample after randomization of the positions is above the dashed line. Less than a third of the low mass haloes are homogeneously distributed. The difference between the dash-dotted and dashed line is much larger for the HM_6 haloes in the right panel, because they are more clustered, and the randomization thus has a proportionally greater effect.

The trend goes in the same direction, but is weaker, for the GL_i samples of galaxies selected by luminosities. There is only limited difference in the distribution of these samples of galaxies with respect to the reference spirals. Position randomization acts in the same way as for the haloes, but the cumulative fraction of the partly randomized test objects

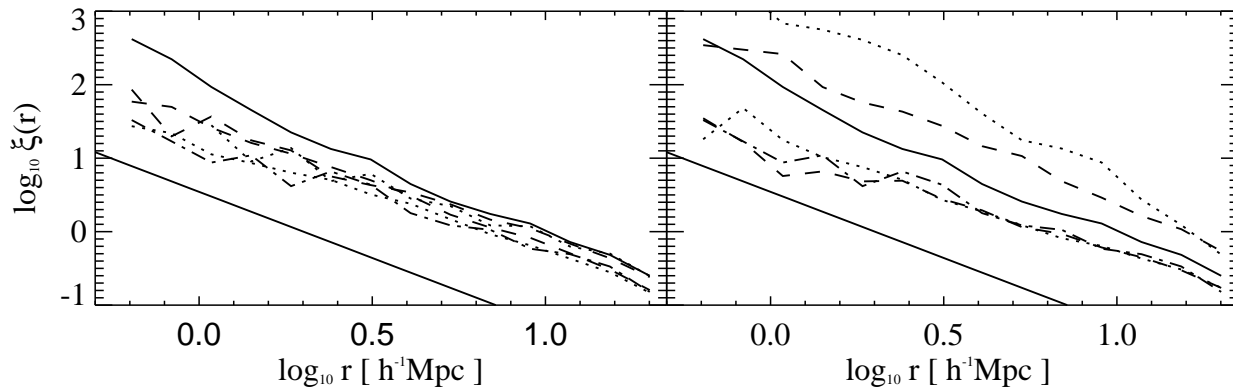


Figure 4. The real-space correlation functions of our samples. The left panel shows the correlation of the HM_1 and GL_1 samples (dotted and dashed lines respectively) and of the HM_5 and GL_5 samples (dotted and dashed lines, above the two previous ones); the right panel gives the correlation functions of the GC_1 and GC_7 samples (dotted lines, with GC_1 below the solid line) and of the GM_1 and GM_7 samples (dashed lines, with GM_1 below the solid line). In both panels, the solid line is the correlation of the dark matter, and the dashed-dotted line that of the reference galaxies. The straight solid line in the lower left corner of each panel shows a -1.8 slope.

is always the highest. Less than a third of even the faintest galaxies is homogeneously distributed.

The colour-selected, blue GC_1 sample would be the best candidate for a population filling the voids between spirals. However, after partly redistributing its population, the distance to the nearest spiral at a given fraction of the objects is still higher than for the initial GC_1 sample. Although the difference between true and randomized samples is somewhat weaker than in the previous cases, the conclusion for a homogeneous population is negative. Note that galaxies in GC_1 also have the highest average SFR per stellar mass (among all colour selected samples), and may be termed “active galaxies”. Conversely, the reddest sample has nearest spiral neighbours clearly closer than have the spirals themselves, consistent with the above results for massive clusters, and the fact that very red galaxies are mostly satellite galaxies of such systems.

The trends in nearest neighbour statistics for the morphologically selected samples (GM_i) are similar to the results obtained for colour selection, but with a somewhat lower amplitude.

A detailed comparison with the observational results presented in P01 is difficult both because the analysis there is carried out in redshift space and, more importantly, because the definition and completeness of the observational samples are difficult to quantify. The qualitative agreement is, however, quite good. The most broadly distributed subsamples in our simulation (e.g. GC_1 , GL_1 or GM_1) have nearest neighbour distributions which relate to those of the reference spirals in much the same way as P01 finds for his observed samples of dwarf and LSB galaxies. In addition, the change in the distributions caused by randomizing the positions of a third of the test galaxies, are similar in the simulated and observed samples. We conclude that the nearest neighbour statistics suggest that the behaviour of the observed and simulated populations with respect to voids are quite similar.

6 CONCLUSIONS

We have looked for signatures of voids in the Λ CDM simulation of M01, which mimics the dark matter and galaxy distribution of the Local Universe up to 8000 km s^{-1} . The simulation can resolve the morphology of an LMC-type galaxy and the luminosity of a dwarf elliptical. We have addressed the question, raised by P01, of whether numerical simulations of galaxy formation in the current standard picture predict objects in the observationally empty spaces defined by normal, L_* spirals.

We showed first that regions of size $\sim 10 h^{-1} \text{ Mpc}$ exist in the simulation which are devoid of even the smallest DM haloes we can resolve. We studied the distribution of galaxies as a function of luminosity, colour and morphology, and the halo distribution as a function of mass. We found that *none* of our samples fills in underdense DM environments. The faint-end slope of the “equal-mass” luminosity functions computed in regions of different densities shows some steepening as one goes to less dense regions: dwarfs are relatively more abundant than L_* galaxies in comparison with high density regions, but the overall variation of the shape of the LF is limited. Nearest neighbour statistics suggest that none of our simulated populations can be considered to fill in the voids defined by L_* spirals. This contrasts with the discussion of P01, who states that at $z=0$ there is still a significant fraction of the matter in regions between clusters and filaments in simulations of a flat, low-density universe. Down to its resolution limit, our scheme of galaxy formation qualitatively reproduces the observed galaxy populations around voids.

The present simple study can be expanded in two ways. First, one might derive a more quantitative comparison based, for instance, on the distribution of the sizes of the voids, which could be compared to the observations of Müller et al. (2000) or to the analytical model of Friedmann & Piran (2001). Second, one can go to higher resolution. However, with current computer capacities, simulations of the size of the one exploited here are already costly. Furthermore,

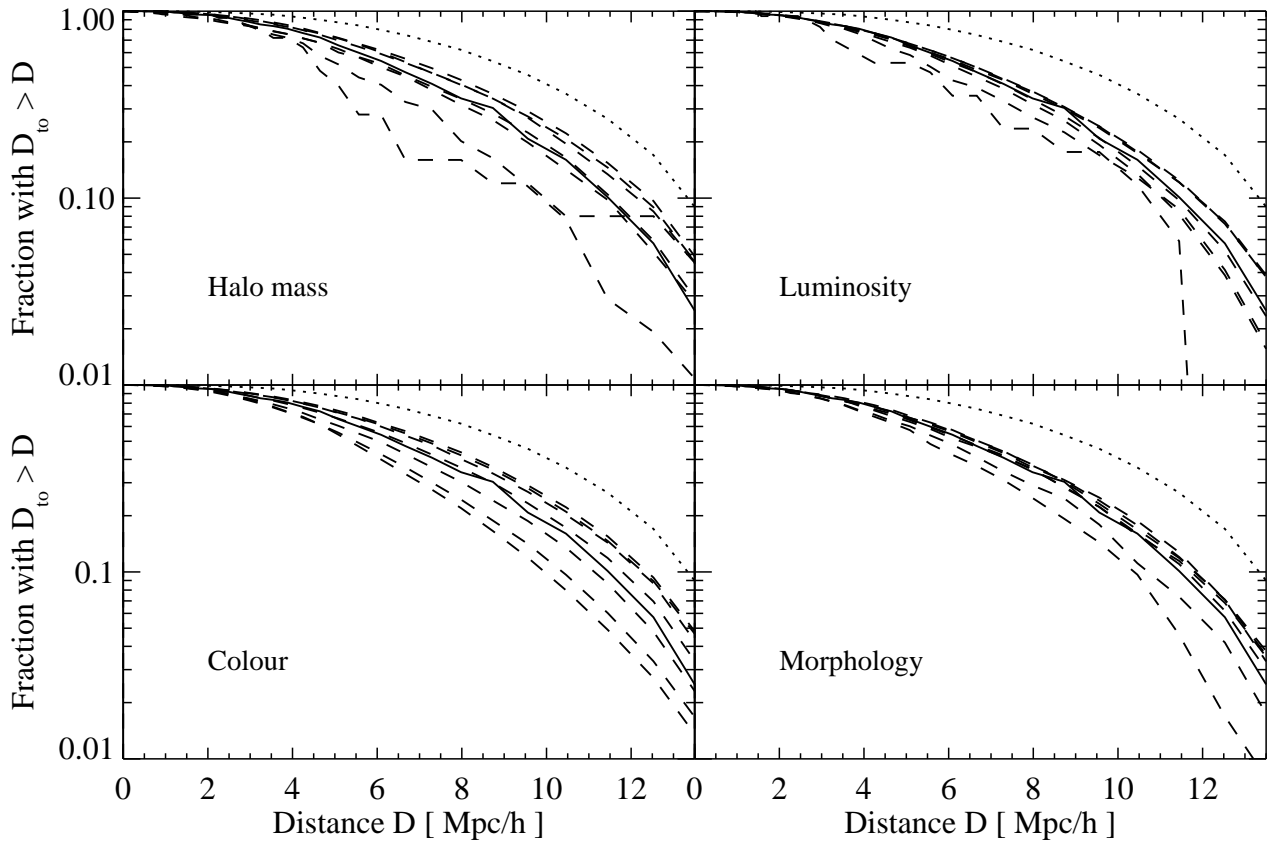


Figure 5. The cumulative distribution of the distances D_{t0} from the test galaxies of the various samples to the nearest reference galaxy (dashed lines), the cumulative distribution of the distances D_{00} from reference galaxies to the nearest other reference galaxy (solid line), and the cumulative distribution of the distances D_{t0} measured from the nodes of a regular mesh to their nearest reference galaxy (dotted line). The sample indices associated with the curves increase from the right to the left.

a comprehensive reevaluation of the relative importance of the physical processes would be needed. For example, nearby ionizing sources at $z \sim 3$ or the general UV background may inhibit the formation of galaxies like the Fornax dwarf in a spatially modulated way.

ACKNOWLEDGEMENTS

The simulations presented in this paper were carried out on the T3E supercomputer at the Computing Center of the Max-Planck-Society in Garching, Germany.

Simulated galaxy populations analysed here are publicly available at

<http://www.mpa-garching.mpg.de/NumCos/CR/>

This paper has been produced using the Royal Astronomical Society/Blackwell Science L^AT_EX style file.

REFERENCES

- Benson A. J., Frenk C. S., Baugh C. M., Cole S., Lacey C. G., 2001a, *MNRAS*, 327, 1041
 Benson A. J., Pearce F. R., Frenk C. S., Baugh C. M., Jenkins A., 2001b, *MNRAS*, 320, 261
 Bode P., Ostriker J. P., Turok N., 2001, *ApJ*, 556, 93
 Bothun G. D., Schombert J. M., Impey C. D., Sprayberry D., McGaugh S. S., 1993, *AJ*, 106, 530
 Cen R., Ostriker J. P., 2000, *ApJ*, 538, 83
 de Vaucouleurs G., de Vaucouleurs A., Corwin H. G., Buta R. J., Paturel G., Fouque P., 1991, *Third reference catalogue of bright galaxies*, Springer-Verlag, New York
 Dey A., Strauss M. A., Huchra J. P., 1990, *AJ*, 99, 463
 Diaferio A., Kauffmann G., Balogh M. L., White S. D. M., Schade D., Ellingson E., 2001, *MNRAS*, 323, 999
 Diaferio A., Kauffmann G., Colberg J. M., White S. D. M., 1999, *MNRAS*, 307, 537
 Dressler A., 1980, *ApJ*, 236, 351
 Eder J. A., Schombert J. M., Dekel A., Oemler A., 1989, *ApJ*, 340, 29
 El-Ad H., Piran T., 1997, *ApJ*, 491, 421
 El-Ad H., Piran T., 2000, *MNRAS*, 313, 553
 El-Ad H., Piran T., da Costa L. N., 1997, *MNRAS*, 287, 790
 Friedmann Y., Piran T., 2001, *ApJ*, 548, 1
 Governato F., Baugh C. M., Frenk C. S., et al., 1998, *Nature*, 392, 359
 Jing Y. P., 1998, *ApJ*, 503, L9
 Kauffmann G., Colberg J. M., Diaferio A., White S. D. M., 1999a, *MNRAS*, 303, 188
 Kauffmann G., Colberg J. M., Diaferio A., White S. D. M., 1999b, *MNRAS*, 303, 188
 Kauffmann G., Colberg J. M., Diaferio A., White S. D. M., 1999c,

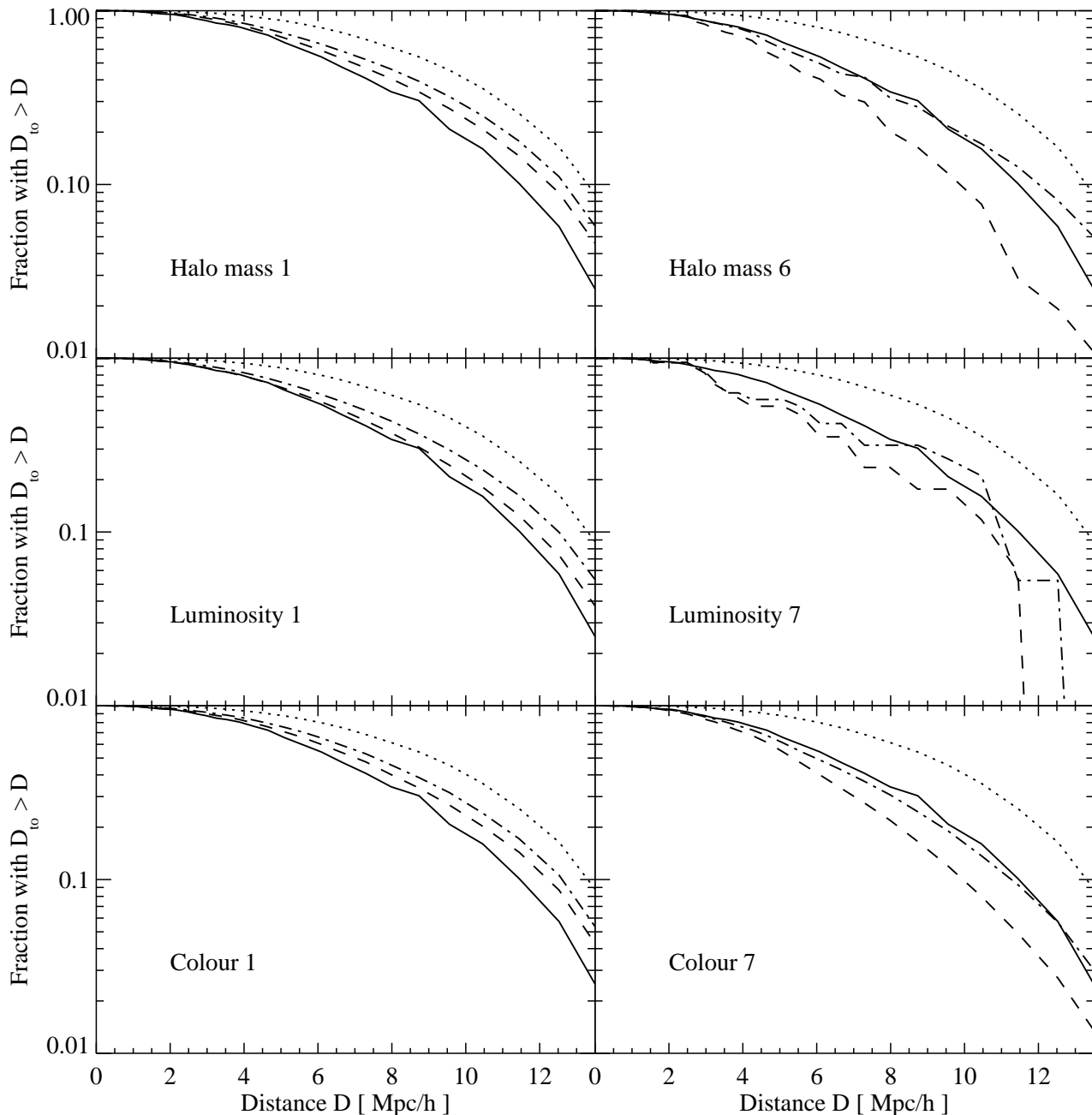


Figure 6. The dashed line gives D_{to} for the extreme bins of each sample (1 and 7, with the exception of HM_6). The dash-dotted lines show the corresponding D_{to} after randomizing the positions of one third of the objects in each test sample, and the solid curve gives D_{oo} . The dotted line is the same as in the previous Figure.

MNRAS, 307, 529
 Kauffmann G., Nusser A., Steinmetz M., 1997, MNRAS, 286, 795
 Kirshner R. P., Oemler A. J., Schechter P. L., Shtetman S. A., 1981, ApJ, 248, 57
 Lee J. C., Salzer J. J., and D. A. Law J. L. R., 2000, ApJ, 536, 606
 Lindner U., Einasto M., Einasto J., et al., 1996, A&A, 314, 1
 Mathis H., Lemson G., Springel V., et al., 2001, preprint, astro-ph/0111099
 Mo H. J., White S. D. M., 1996, MNRAS, 282, 347
 Müller V., Arbabi-Bidgoli S., 2001, Progress in Astronomy, 19,

28
 Müller V., Arbabi-Bidgoli S., Einasto J., Tucker D., 2000, MNRAS, 318, 280
 Peebles P. J. E., 1989, J. Roy. Astron. Soc. Can., 83, 363
 Peebles P. J. E., 2001, ApJ, 557, 495
 Peebles P. J. E., Phelps S. D., Shaya E. J., Tully R. B., 2000, ApJ, 554, 104
 Plionis M., Basilakos S., 2001, preprint, astro-ph/0106491
 Pustil'nik S. A., Ugryumov A. V., Lipovetski V. A., Thuan T. X., Guseva N. G., 1995, ApJ, 443, 499
 Rees M. J., 1985, MNRAS, 213, 75

- Salzer J. J., Hanson M. M., Gavazzi G., 1990, ApJ, 353, 39
Simien F., de Vaucouleurs G., 1986, ApJ, 302, 564
Somerville R. S., Primack J. R., Faber S. M., 2001, MNRAS, 320, 504
Soneira R. M., Peebles P. J. E., 1977, ApJ, 211, 1
Springel V., White S. D. M., Tormen G., Kauffmann G., 2001, MNRAS, 328, 726
Srianand R., 1997, ApJ, 478, 511
Szomoru A., van Gorkom J. H., Gregg M. D., 1996a, AJ, 111, 2141
Szomoru A., van Gorkom J. H., Gregg M. D., Strauss M. A., 1996b, AJ, 111, 2150
Thoul A. A., Weinberg D. H., 1996, ApJ, 465, 608
Tully R. B., 1988, *Nearby galaxies catalogue*, Cambridge: Cambridge University Press
Vogeley M. S., Geller M. J., Park C., Huchra J. P., 1994, AJ, 108, 745
White S. D. M., Frenk C. S., Davis M., Efstathiou G., 1987, ApJ, 313, 505
Willmer C. N. A., da Costa L. N., Pellegrini P. S., 1998, AJ, 115, 869

This figure "Figure1.gif" is available in "gif" format from:

<http://arxiv.org/ps/astro-ph/0201193v1>